Springer

KSME

Journal of Mechanical Science and Technology 32 (9) (2018) 4125~4134
www.springerlink.com/content/1738-494x(Print)/1976-3824(Online)
DOI 10.1007/s12206-018-0810-8

A novel negative dislocated seal and influential parameter analyses of static/rotordynamic characteristics †

Dan Sun[1], Xudong Wang[1], Chengwei Fei[2,*], Shuang Wang[1] and Yanting Ai[1]

[1]*Liaoning Key Lab of Advanced Test Technology for Aerospace Propulsion System, Shenyang Aerospace University, Shenyang 110136, China*
[2]*School of Transportation Science and Engineering, Beihang University, Beihang 100191, China*

(Manuscript Received February 28, 2018; Revised May 4, 2018; Accepted May 9, 2018)

Abstract

This paper proposes a new type of negative dislocated seal (NDS) based on the dislocated bearing theory to investigate the influential parameters of static rotor eccentricity and dislocated ratio on the static and rotordynamic characteristics of an example seal solved with computational fluid dynamics (CFD) the flow field. The rotordynamic characteristics of the NDS were investigated in respect of the effects of rotor whirling frequency on response force, stiffness coefficients, damping coefficients and rotor system stability, by multi-frequency elliptical orbit rotor whirling model. Based on the studies, we reached the following conclusions. The circumferential pressure distribution of NDS and conventional labyrinth seal (LS) presents sine periodic variation approximately, while relative to the LS, the NDS has two divergent wedge gaps and reduces the hydrodynamic pressure effects, then the circumferential pressure difference and tangential force on rotor surface decreases by about 40 %~190 %. The leakage of the NDS linearly increases with the rising eccentricity ratio and dislocation ratio approximately, and is larger (about 0.9 %~1.5 %) than the LS. The direct stiffness coefficients of the two seals increase with the rise of rotor whirling frequency, while the absolute values of both the cross-coupled stiffness coefficients and the damping coefficients decrease with raising rotor whirling frequency. Compared with the LS, the NDS has smaller (about 28.8 %~206.2 %) cross-coupled stiffness coefficient, larger (about 26.15 %~60.39 %) effective damping coefficient, and good stability of rotor system. This study has developed a novel seal structure to improve the seal performance of turbomachinery such as aeroengine.

Keywords: Negative dislocated seal; Multi-frequency whirling model; Static characteristics; Rotordynamic characteristics; Rotor system stability

1. Introduction

The seal, which is the key component of turbomachinery, such as aeroengine, is used to increase work efficiency by reducing internal leakage through the clearances between a rotor and a stator from a high-pressure region to a low-pressure region [1-3]. Labyrinth seal (LS) is the most common type of seal. Herein, the static and rotordynamic characteristics of LS seriously influence the work efficiency and rotordynamic stability of turbomachinery with high rotational speed, operating under high pressure environment [4-6].

There are currently two commonly used types of seals in turbomachinery to reduce seal destabilizing force. One is the anti-preswirl seal. According to engineering practice, fluid preswirl rate influences the seal rotordynamic characteristics, and the seal cross-coupled stiffness coefficients generated by fluid preswirl rate cause the unsteadiness of rotor. To increase rotordynamic stability, the swirl vanes at the inlet of the seal are used as small inlet/outlet pressure difference or short seal axial length [7, 8]. The swirl vanes effectively reduce fluid preswirl rate and seal cross-coupled stiffness coefficient. Nielsen [9] and Sun [10] validated that swirl vanes are promising to reduce fluid preswirl rate and improve the rotor system stability through experiments. Baldassare et al. [11] evaluated the effects of geometrical parameters on swirl brake performance using numerical and experimental methods. Shunt injection, by which high-pressure gas is injected into an intermediate labyrinth cavity at several circumferential locations to reduce preswirl rate, is also a proven approach to improve the rotordynamic stability of the traditional LS [12-14], but its major disadvantage is large fluid loss in some cases [15]. The other is damper seal, which was first proposed by Von Pragenau [16]. Damper seals (honeycomb [17], hole-pattern [18] and pocket damper seal [19]) increase the effective damping by changing the roughness of the sealing structure to improve the stability of rotor system. All of the above seals are cylinder shape. Under the condition of the eccentric rotor, high pressure and high rotational speed enhance the hydrodynamic pressure effects [20], and then enlarge the response force until the rotor system unstable.

*Corresponding author. Tel.: +852 54249709, Fax.: +852 2358 1543
E-mail address: feicw544@163.com
† Recommended by Associate Editor Doo Ho Lee

As for the numerical approach of seal rotordynamic characteristics, the bulk-flow models were commonly used to predict the seal rotordynamic characteristics in the past. However, the bulk-flow models have some limitations. For instance, the bulk-flow models ignore flow details and largely depend on the empirical parameters, such as flow coefficients and friction factors determined by seal geometry and operating conditions [21]. To overcome the shortcomings, CFD-based methods get increasing attention. Toshio et al. [22] used the CFD moving rotating frame method to solve the seal rotordynamic coefficients, but an important limitation for the CFD moving rotating frame model is that the seal geometry has to be axisymmetric, and this method does not consider the effect of rotor whirling frequency on seal rotordynamic characteristics [23]. Ertas [24] proved that rotor whirling frequency seriously influences seal rotordynamic characteristics by experiments. Yan [25], Chocgua [26], Nielsen [27] and Sreedharan [28] established single-frequency rotor whirling model, and analyzed the laws of seal rotordynamic characteristic coefficients with the variation of rotor whirling frequency under three types of rotor whirling orbits (one-dimensional, circular and elliptical whirling). However, to obtain rotordynamic coefficients under different rotor whirling frequencies, the rotor single-frequency whirling orbit model has to be solved repeatedly, and thus it is inevitable that this model has low computational efficiency. In this case, Li [29] investigated rotor multi-frequency whirling orbit model, to obtain rotordynamic coefficients in multiple whirling frequencies by two unsteady solutions.

For the enhancement problem of seal hydrodynamic pressure effects, we propose a new negative dislocated seal (NDS) based on the principle of dislocated bearing. The NDS possesses two convergent wedge gaps to strengthen the hydrodynamic pressure effect on the positive dislocated bearing. The NDS with two divergent wedge gaps decreases seal air-induced force because this seal cannot form the hydrodynamic pressure effects. We apply the multi-frequency elliptical orbit rotor whirling model to predict the seal rotordynamic characteristics. We then analyze the impacts of eccentricity ratio, whirling frequency and dislocation ratio on seal leakage, pressure distribution, response force and rotordynamic coefficients are discussed too.

The rest of this paper is organized as follows. Sec. 2 introduces the concept and mechanism of the developed NDS. The computational method of evaluating the NDS static/ rotordynamic characteristics is discussed in Sec. 3. In Sec. 4 we investigate the static/rotordynamic characteristics of the NDS. Some conclusions are summarized in Sec. 5.

2. Negative dislocated seal

According to field troubleshooting experiences, the tangential force generated by the LS is the major mechanism inducing a load-dependent instability vibration [7]. The seal tangential force is generated due to asymmetrical circumferential

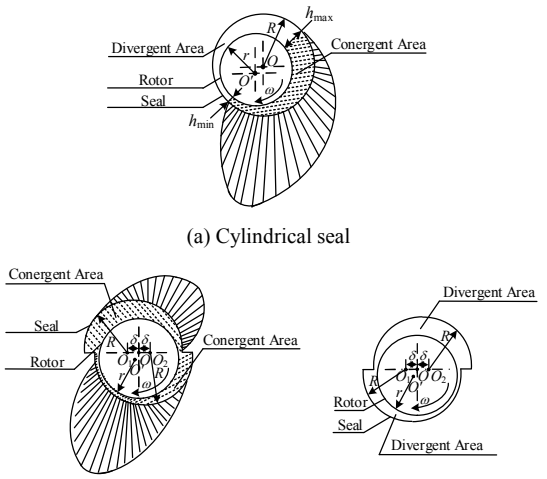

(a) Cylindrical seal

(b) Positive dislocated seal (c) Negative dislocated seal

Fig. 1. Schematic diagram of cylindrical and dislocated seal hydrodynamic pressure effects.

pressure distribution under the condition of eccentric rotor. The flow field between both seal stator and rotor is similar to that between the journal bearing stator and rotor, as the rotor eccentrically rotates with a high speed. Seal and journal bearing with an eccentric rotor can form the hydrodynamic pressure effects when the viscous fluid flows from the big terminal to the small terminal of the wedge gap.

To intensify the hydrodynamic pressure effects akin to a journal bearing, the dislocated journal bearing is applied in large-scale rotating machinery. The positive dislocated journal bearing makes the fluid flows from big terminal to the small terminal of the wedge gap in two oil wedge, so that the hydrodynamic pressure effect more obvious.

Based on the principle of dislocated bearings, Fig. 1 shows the schematic diagram of hydrodynamic pressure effect of seals. In Fig. 1, O and O' are the seal center and rotor center, respectively. The stator centers of dislocated seal are O_1 and O_2, respectively. The structure parameters of the cylinder seals and dislocated seals contain seal radius R, rotor radius r, the distance δ between the stator center and the center of the dislocated seal, the maximum clearance h_{max} of the seal, the minimum clearance h_{min} of the seal. The rotational speed of rotor is ω.

As shown in Fig. 1(a), the traditional cylindrical seal can form the hydrodynamic pressure effect in the area of convergent air wedge under the condition of eccentric rotor, while the hydrodynamic pressure effect does not exist in the area of divergent air wedge.

Compared with the traditional cylindrical seal, the stator horizontal middle plane of the dislocated seal is staggered and it includes both positive dislocated and negative dislocated forms. As demonstrated in Fig. 1(b), the fluid in the positive dislocated seal flows from big terminal to small terminal in the seal wedge gap, and forms an intensive hydrodynamic pressure effect. A structural diagram of the developed NDS is

Table 1. Seal dimensions and operating conditions.

No. of teeth	5
Rotation speed (r·min^{-1})	11097
Fluid	Ideal gas
Turbulence model	k-ε
Inlet p (Pa)	3.447×10^6
Outlet p (Pa)	1.724×10^6
Inlet temperature (K)	366.7
Inlet swirl (m·s^{-1})	0
Seal length (mm)	18.796
Radial inlet clearance (mm)	0.292
Seal inner diameter (mm)	275.384

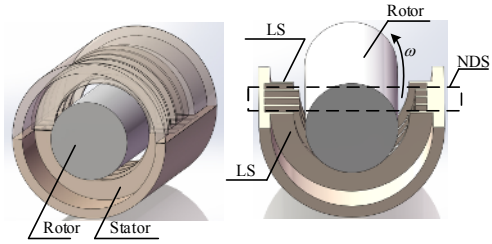

Fig. 2. Structure diagram of the developed NDS.

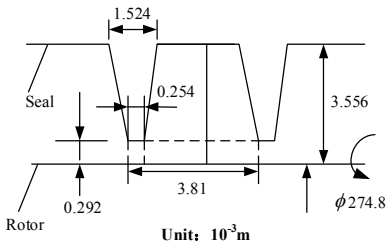

Fig. 3. Dimensions of the seal.

shown in Fig. 2, and as demonstrated in Fig. 1(c), the NDS can suppress the seal hydrodynamic pressure effects because it has two divergent wedge gaps. Therefore, the NDS improves the rotor system stability.

3. Numerical approach

3.1 Computational model

In this paper, the computational model of the conventional LS is from the Ref. [22]. Table 1 shows the seal geometrical parameters and operational conditions in the CFD analyses.

The seal consists of a rotor with smooth surface and a stator with five teeth. Fig. 3 shows the used dimensions of the seal in this calculation. The static/rotordynamic characteristics for the new NDS were analyzed under three dislocation ratios, four eccentricity ratios and five whirl frequencies. The dislocation ratio γ is defined as

$$\gamma = \frac{\delta}{R-r}. \tag{1}$$

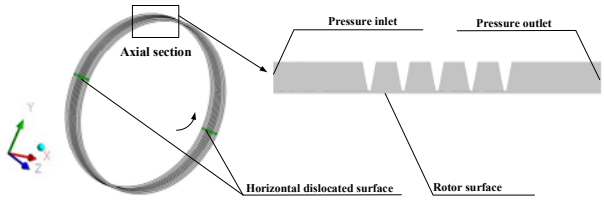

Fig. 4. Schematic diagram of seal model boundary condition.

In this work, the full eccentric 3D CFD computational meshes were constructed. For the negative dislocated seal, the upper and lower parts of the horizontal dislocated surface are made of hexahedral mesh, and the horizontal dislocated surfaces adopt the boundary condition of interface. Based on the grid density analysis for the leakage, the grid number is determined as 2.75 million. The Reynolds-averaged-Navier-Stokes (RANS) CFD analysis in the whole flow field was solved by ANSYS CFX 16.0 software.

Fig. 4 shows the boundary conditions of the NDS. The pressures at inlet and outlet boundaries are given. The rotor surface has a circumferential velocity. The dislocated horizontal planes of the NDS adopt the boundary condition of interface.

3.2 Rotor multi-frequency whirling model

We applied the multi-frequency elliptical orbit whirling model to analyze the influence of rotor whirling frequency on seal rotordynamic characteristics, two separate transient solutions are applied to obtain the seal rotordynamic coefficients for each rotor whirling frequency. The multi-frequency elliptical orbit whirling motion of the rotor is described by Eqs. (2) and (3).

$$\begin{cases} x = A\cdot\sum_{i=1}^{N}\cos(\Omega_i t) \\ y = B\cdot\sum_{i=1}^{N}\sin(\Omega_i t) \end{cases} \tag{2}$$

$$\begin{cases} x = B\cdot\sum_{i=1}^{N}\cos(\Omega_i t) \\ y = A\cdot\sum_{i=1}^{N}\sin(\Omega_i t) \end{cases} \tag{3}$$

where N is the number of the rotor whirling frequencies, $\Omega_i = 2\pi f_i$ is whirling angular velocity, f_i is the rotor whirling frequency (i = 1, 2, 3…).

Fig. 5 gives the multiple-frequency elliptical orbit whirling of the rotor when N = 5, $A = 2B$ = 2.92 um, f_i = 40 Hz, 80 Hz, 120 Hz, 160 Hz, 200 Hz. To satisfy the small motion theory, the maximum displacement should be less than 10 % of the seal clearance [30], hence the motion amplitude (for each frequency component) is set to be $A = 0.01C_r$ and $B = 0.005C_r$,

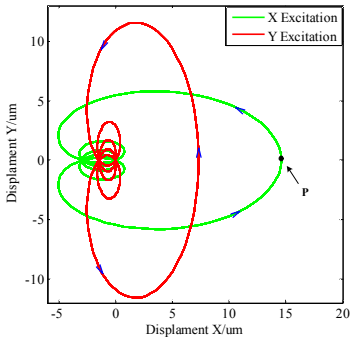

Fig. 5. Multiple-frequency elliptical orbit whirling of the rotor.

in which C_r is sealing clearance.

3.3 Seal rotordynamic coefficients identification technique

When the rotor is disturbed by a small displacement and velocity, the relationship between the two response forces along the X and Y directions and the dynamic displacements and velocities can be expressed by a linear equation:

$$-\begin{bmatrix}\Delta F_x\\ \Delta F_y\end{bmatrix}=\begin{bmatrix}K_{xx} & K_{xy}\\ K_{yx} & K_{yy}\end{bmatrix}\begin{bmatrix}\Delta x\\ \Delta y\end{bmatrix}+\begin{bmatrix}C_{xx} & C_{xy}\\ C_{yx} & C_{yy}\end{bmatrix}\begin{bmatrix}\Delta \dot{x}\\ \Delta \dot{y}\end{bmatrix} \tag{4}$$

where $K_{mn}(m, n = x, y)$ and $C_{mn}(m, n = x, y)$ represent the stiffness and damping coefficients of the seal, respectively; Δx, Δy, $\Delta \dot{x}$ and $\Delta \dot{y}$ are the dynamic displacements and velocities along the X and Y directions, respectively.

To obtain the seal rotordynamic characteristics for each rotor whirling frequency, the fast Fourier transform (FFT) algorithm is applied to transform Eq. (4) into the algebraic set:

$$\begin{cases}-\Delta F_x=(K_{xx}+j\Omega C_{xx})\cdot D_x+(K_{xy}+j\Omega C_{xy})\cdot D_y\\ -\Delta F_y=(K_{yy}+j\Omega C_{yy})\cdot D_y+(K_{yx}+j\Omega C_{yx})\cdot D_x\end{cases} \tag{5}$$

where $j=\sqrt{-1}$, (D_x, D_y) and $(\Delta F_x, \Delta F_y)$ are complex numbers containing multi-frequency components.

In line with the transient CFD analysis, we can gain whirling displacements and response forces in a time domain. To obtain the eight rotordynamic coefficients, the multi-frequency elliptical orbit whirling of the rotor is governed by Eqs. (2) and (3), respectively. Both four independent equations and four unknown quantities are defined in Eqs. (6) and (7).

$$\begin{cases}-\Delta F_{xx}=(K_{xx}+j\Omega C_{xx})\cdot D_{xx}+(K_{xy}+j\Omega C_{xy})\cdot D_{xy}\\ -\Delta F_{xy}=(K_{yy}+j\Omega C_{yy})\cdot D_{xy}+(K_{yx}+j\Omega C_{yx})\cdot D_{xx}\end{cases} \tag{6}$$

$$\begin{cases}-\Delta F_{yy}=(K_{yy}+j\Omega C_{yy})\cdot D_{yy}+(K_{yx}+j\Omega C_{yx})\cdot D_{yx}\\ -\Delta F_{yx}=(K_{xx}+j\Omega C_{xx})\cdot D_{yx}+(K_{xy}+j\Omega C_{xy})\cdot D_{yy}\end{cases} \tag{7}$$

where D_{uv} and F_{uv} are the whirling displacement in excitation direction u and the response force in direction v.

The impedance coefficients of the seal are

$$\begin{cases}H_{xx}=K_{xx}+j\Omega C_{xx}\\ H_{xy}=K_{xy}+j\Omega C_{xy}\\ H_{yx}=K_{yx}+j\Omega C_{yx}\\ H_{yy}=K_{yy}+j\Omega C_{yy}\end{cases}. \tag{8}$$

Inputting Eq. (8) into Eqs. (6) and (7), the impedance coefficients can be gained as

$$\begin{cases}H_{xx}=\dfrac{(-F_{xx})\cdot D_{yy}-(-F_{yx})\cdot D_{xy}}{D_{xx}\cdot D_{yy}-D_{yx}\cdot D_{xy}}\\ H_{xy}=\dfrac{(-F_{xx})\cdot D_{yx}-(-F_{yx})\cdot D_{xx}}{D_{xy}\cdot D_{yx}-D_{yy}\cdot D_{xx}}\\ H_{yy}=\dfrac{(-F_{yy})\cdot D_{xx}-(-F_{xy})\cdot D_{yx}}{D_{yy}\cdot D_{xx}-D_{yx}\cdot D_{xy}}\\ H_{yx}=\dfrac{(-F_{yy})\cdot D_{xy}-(-F_{xy})\cdot D_{yy}}{D_{xy}\cdot D_{yx}-D_{yy}\cdot D_{xx}}\end{cases}. \tag{9}$$

Then, the stiffness coefficients and damping coefficients are corresponding to the real parts and image parts of H_{mn}, respectively:

$$\begin{cases}K_{xx}=\mathrm{Re}(H_{xx})\\ K_{xy}=\mathrm{Re}(H_{xy})\\ K_{yx}=\mathrm{Re}(H_{yx})\\ K_{yy}=\mathrm{Re}(H_{yy})\\ C_{xx}=\dfrac{\mathrm{Im}(H_{xx})}{\Omega}\\ C_{xy}=\dfrac{\mathrm{Im}(H_{xy})}{\Omega}\\ C_{yx}=\dfrac{\mathrm{Im}(H_{yx})}{\Omega}\\ C_{yy}=\dfrac{\mathrm{Im}(H_{yy})}{\Omega}\end{cases}. \tag{10}$$

3.4 Transient response solution method

In this section, the relationship between rotordynamic characteristics and rotor whirling frequency is investigated in view of multi-frequency ellipse whirling model based on unsteady dynamic grid method. This analysis considers five rotor whirling frequencies of [40 Hz, 80 Hz, 120 Hz, 160 Hz, 200 Hz]. To accurately capture rotor whirling displacement and response force, the sampling frequency must be greater than twice the maximum whirling frequency (200 Hz) of rotor according to the sampling principle, and enough data points of rotor whirling displacement and response forces are required in the same time. The sampling frequency is thus determined

Table 2. The comparison of leakage.

	Leakage (kg/s)	Error (%)
CFX-Tascflow [22]	1.08	0.93
CFX	1.09	

Table 3. The comparison of seal stiffness.

	Stiffness coefficients, 10^6 (N/m)			
	K_{xx}	K_{xy}	K_{yx}	K_{yy}
CFX-Tascflow [22]	1.88	-0.72	0.72	1.88
CFX	1.95	-0.78	0.76	1.90
Errors (%)	3.72	8.33	5.56	1.06

Table 4. The comparison of seal dimpling.

	Damping coefficients, 10^3 (Ns/m)			
	C_{xx}	C_{xy}	C_{yx}	C_{yy}
CFX-Tascflow [22]	1.60	1.24	-1.24	1.60
CFX	1.69	1.28	-1.27	1.72
Errors (%)	5.63	3.23	2.42	7.50

as 10000 Hz. The steady state solution is first obtained by only considering rotor spinning and its convergence condition (the root mean square residual of 10^{-6}) for the continuity equation, momentum equation and turbulence equation. The results of the steady flow calculation are taken as the initial value for the unsteady flow calculation considering rotor spinning and whirling motion. The convergence conditions for the unsteady flow calculation are that the residuals of the momentum equation and turbulence equation are less than 10^{-5}, response forces F_x and F_y fluctuate periodically and their change in magnitude is less than 0.2 % when the rotor moves to the same position in two adjacent fundamental period cycles.

4. Parameters analysis of static/rotordynamic characteristics of the NDS

4.1 Verification of numerical method

Table 2 shows the results of seal leakage obtained by CFX and CFX-Tascflow [22], which indicates the relative error of seal leakage between the two methods is 0.93 %. Tables 3 and 4 show the error of rotordynamic coefficients relative to the CFX-Tasc-flow. As shown in Tables 3 and 4, the rotordynamic coefficients by CFX show good agreement with the results by CFX Tasc-flow using the moving rotating frame model in the Ref. [22]. All the relative errors for the eight rotordynamic coefficients are less than 10 % between the two numerical methods. Therefore, the presented CFD model is accurate in predicting the static and rotordynamic characteristics of the seal.

4.2 Steady flow characteristics analyses

Flow field To analyze the sealing principle of the developed NDS, the scattergram of velocity vector of the seal flow field axial profile is shown in Fig. 6. And the pressure of seal flow field along the axial direction is drawn in Fig. 7.

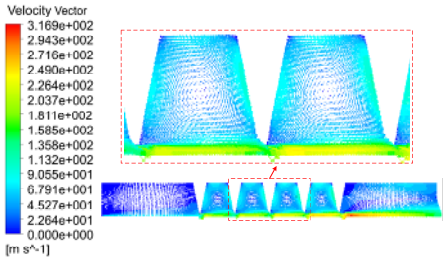

Fig. 6. Scattergram of velocity vector.

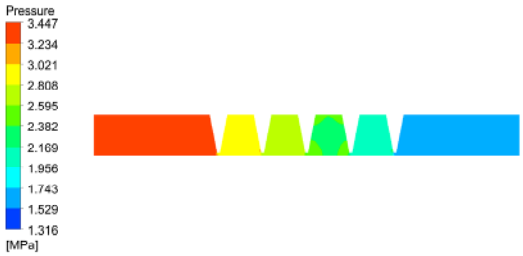

Fig. 7. Static pressure along axial section.

As shown in Figs. 6 and 7, the seal flow field is divided into two parts of the swirl area into the chamber and the jet area at the tip of the tooth; the pressure of the seal flow field decreases stepwise along the axial direction of seal, and drops at the tip of the tooth while is essentially same in the chamber.

Sealing principle As seen in the velocity vector and pressure distribution of the seal flow field, the sealing principle is obtained. A number of ring teeth are arranged on the seal in sequence. When the airflow passes through each of the teeth, the flow section at the tip of the tooth is small so that the velocity of airflow increases rapidly and then the pressure energy of the airflow is turned into kinetic energy. As the airflow enters chamber, the flow velocity of air decreases suddenly because the flow section of the chamber is larger than the top of the tooth. Meanwhile the airflow expands rapidly and produces a strong vortex, and most of the kinetic energy of the airflow is converted into heat energy to lose. The throttling action across a tooth and the kinetic energy dissipation within a cavity result the decrease in pressure and the sealing effect.

Leakage performance Through the comparison of leakage under two seals with the eccentricity ratio varying from 0.1 to 0.7 and the dislocation ratio changing from 0 to 0.7, the eccentricity is parallel to the dislocated direction. The effects of eccentricity ratio on the leakage of seals with different dislocation ratios are drawn in Fig. 8.

As illustrated in Fig. 8, the seal leakage of the traditional LS and the proposed NDS linearly increases approximately with the increase of eccentricity. In the same eccentricity ratio, the seal leakage increases with the increasing dislocation ratio. Besides, the leakage of the NDS is larger (about 0.9 %~1.5 %) than the conventional LS.

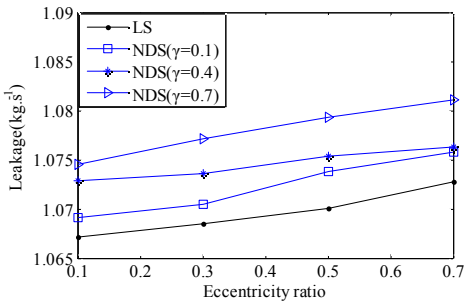

Fig. 8. Effect of eccentricity ratio on the seal leakage.

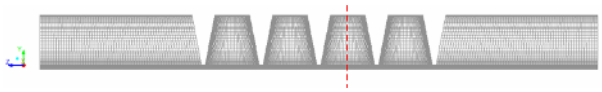

Fig. 9. Sketch map of seal circumferential pressure extraction location.

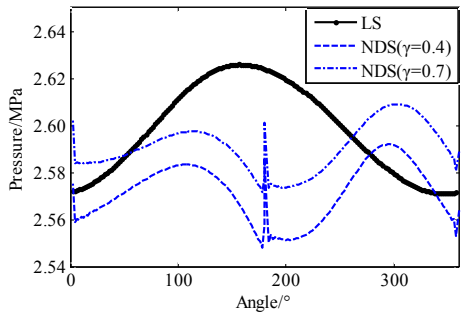

Fig. 10. Circumferential pressure distributions of traditional and new dislocated seals.

Circumferential pressure distribution To study the effect of the dislocation ratio on the circumferential pressure distribution, the central section in second cavity of the eccentric seal is selected as shown in Fig. 9. The circumferential pressure distribution under different dislocation ratios and circumferential angles for the conventional LS and the new NDS are drawn in Fig. 10 when the rotor eccentricity is 0.5. Herein, the 0 degree is defined as the dislocation position of horizontally middle plane along the *x* direction.

As shown in Fig. 10, (1) the circumferential pressure distributions of the seals with or without dislocation vary approximate to sinusoid; (2) the circumferential pressure breakpoint in the dislocated seal appears at the horizontal dislocation; (3) the pressure of the LS changes from 2.571 MPa to 2.626 MPa with the pressure difference 0.055 MPa, while the pressure of the new NDS (dislocation ratio of 0.4) varies from 2.548 MPa to 2.592 MPa with the difference is 0.044 MPa; (4) The pressure difference of the seal decreases with the increasing of dislocation ratio.

Tangential force The NDS applied to suppress the seal hydrodynamic pressure effects should reduce the destabilizing tangential force. Considering the eccentricity ratio varying from 0.1 to 0.7 and the dislocation ratio changing from 0 to 0.7, the tangential forces of both LS and NDS versus eccentricity ratio are illustrated in Fig. 11.

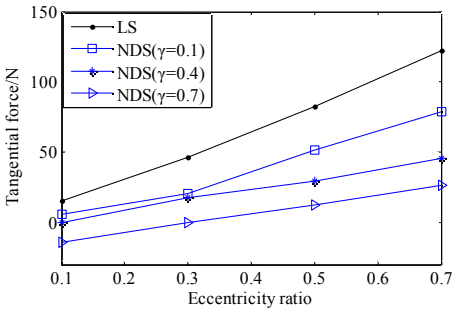

Fig. 11. Effect of eccentricity ratio on the seal tangential force.

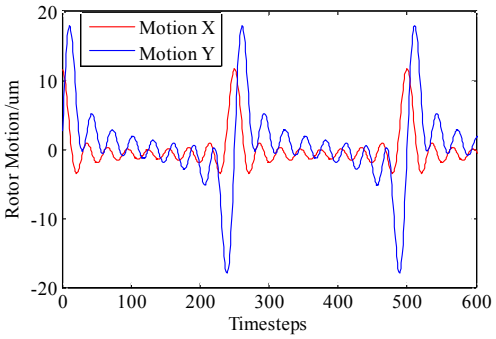

(a) Time domain whirling displacement

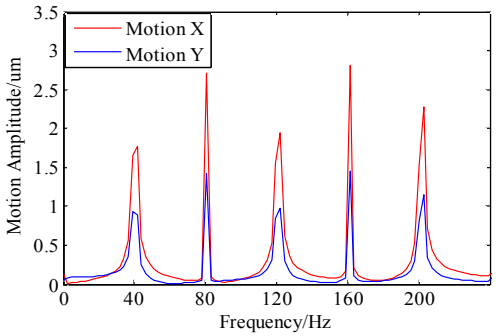

(b) Frequency domain whirling displacement

Fig. 12. The diagram of rotor whirling displacement.

As demonstrated in Fig. 11, (1) the seal tangential force is approximately equal to 0 pertaining to small eccentricity ratios and increases with the rise of eccentricity ratio; (2) the difference of two seal tangential forces increase with the rising eccentricity ratio and dislocation ratio; (3) the tangential force with the NDS decreases by 40 %~190 % relative to the traditional LS. Therefore, the NDS dramatically reduces the seal tangential forces under ensuring the efficiency of rotating machinery.

4.3 Rotordynamic characteristics

Influence of rotor whirling frequency on response force Based on the effect analysis of rotor whirling frequency on response force, the time series displacements of rotor whirling and the corresponding Fourier transform are drawn in Fig. 12.

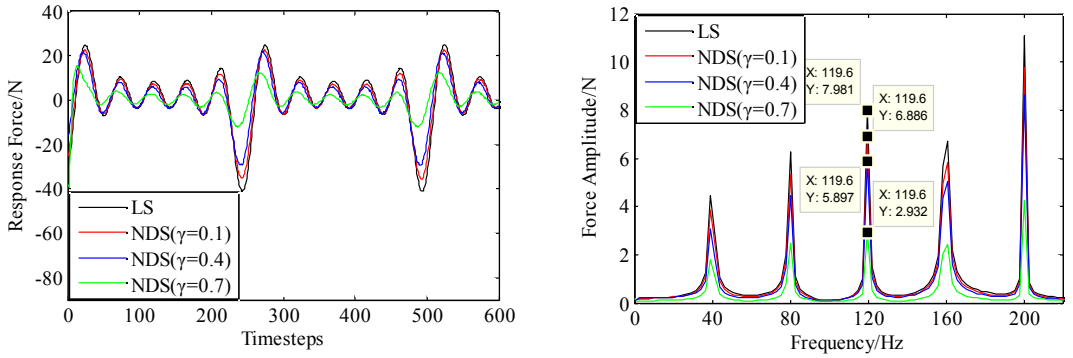

(a) Time domain response force (b) Frequency domain response force

Fig. 13. Time domain and frequency domain of response force.

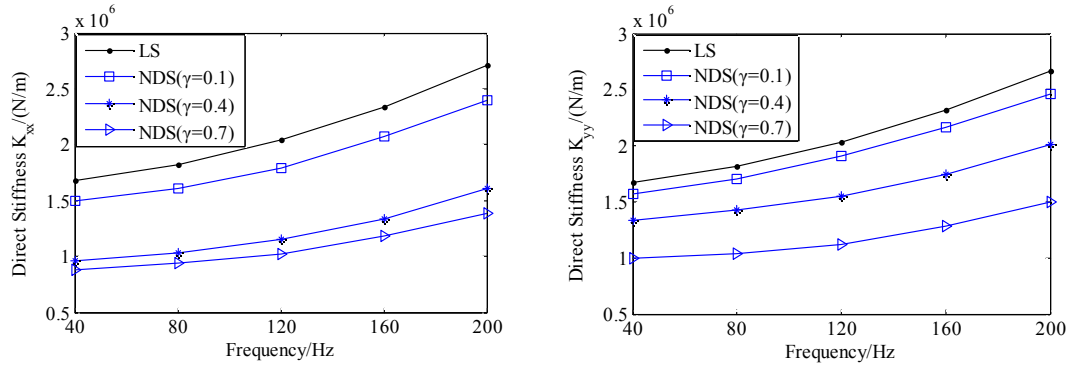

(a) Direct stiffness coefficients

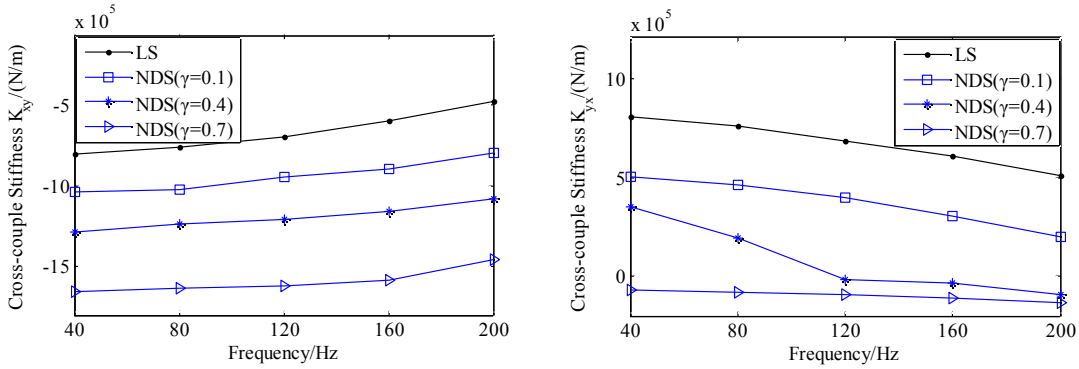

(b) Cross-coupled stiffness coefficients

Fig. 14. Variation of different stiffness coefficients with rotor whirling frequency.

In Fig. 12, the motion amplitude and frequency calculated by the multi-frequency method are similar to the set in Eq. (3). Therefore, the multi-frequency method is effective in simulating the multi-frequency complex motion of the rotor.

Fig. 13 shows the time domain graph and frequency domain graph of the response forces when the rotor eccentricity is 0. As demonstrated in Fig. 13, (1) the response force changing with frequencies obtained by multi-frequency method are the same as the frequencies of the rotor whirling, and increases with the increase of the rotor whirling frequency for the same motion amplitude; (2) all the response force for the NDS is lower than that for the LS in each rotor whirling frequency, and decreases with the increase of the dislocation ratio; (3) the developed NDS is more effective in reducing response force than the LS.

Influence of rotor whirling frequency on rotordynamic coefficients Through the analysis, the relationship between rotor whirling frequency and rotordynamic coefficients when the rotor eccentricity is 0 is drawn in Figs. 14 and 15.

As shown in Figs. 14 and 15, (1) the rotor whirl frequency strongly influences both stiffness coefficients and damping coefficients; (2) the direct stiffness coefficients of both LS and the NDS increase with the rise of rotor whirling frequency, while the absolute values of both cross-coupled stiffness coef-

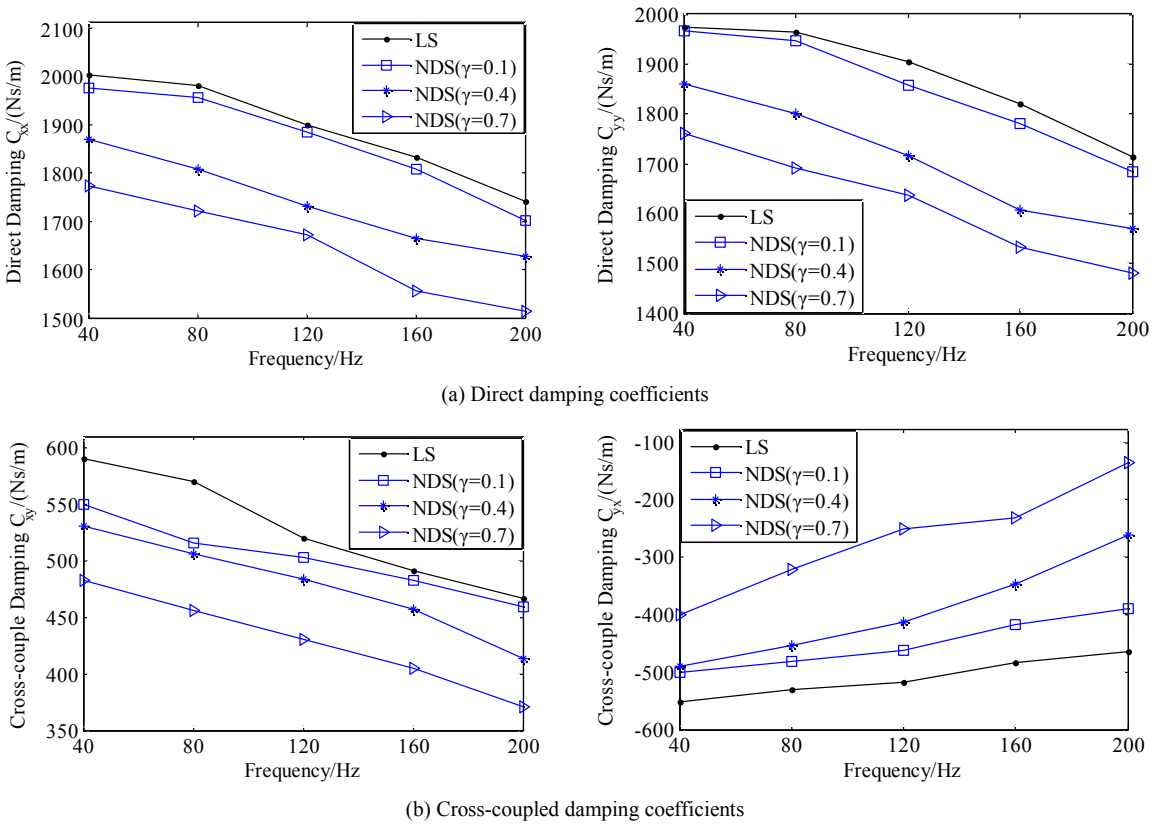

(a) Direct damping coefficients

(b) Cross-coupled damping coefficients

Fig. 15. Variation of damping coefficients with rotor whirling frequency.

ficients and damping coefficients decrease with the raising rotor whirling frequency; (3) in the same rotor whirling frequency, the cross-coupled stiffness coefficient of the NDS is smaller (about 28.8 %~206.2 %) than the LS; and (4) large dislocation ratio leads to the reduction of the cross-coupled stiffness coefficients.

4.4 Rotor system stability

For a small amplitude processional motion, both the stabilizing effect of the direct damping coefficient C_{xx} and the destabilizing forces developed by the cross-coupled stiffness coefficient K_{xy} commonly determine the effective damping coefficient C_{eff} [21] expressed as

$$C_{eff} = C_{xx}(\Omega) - K_{xy}(\Omega)/\Omega . \tag{11}$$

Fig. 16 shows the relationship between effective damping coefficients and rotor whirling frequencies by solving Eq. (11). As displayed, the effective damping coefficient decreases with the increasing rotor whirling, and the negative dislocated structure of the NDS makes effective damping coefficients larger (about 26.15 %~60.39 %) than the circular structure of the LS, especially the large dislocation ratio. Therefore, the NDS is more stable than the LS.

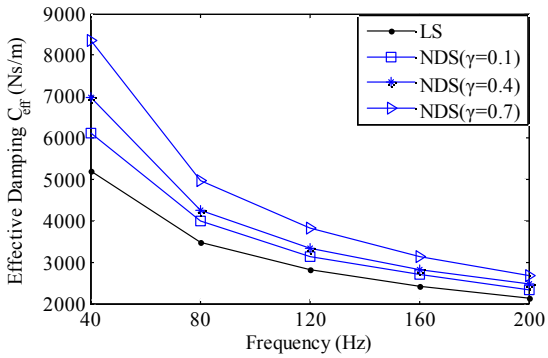

Fig. 16. Variation of effective damping coefficients with rotor whirling frequencies.

5. Conclusions

We have presented a new, negative dislocated seal (NDS) according to the dislocated bearing principle. The impacts of eccentricity ratio, dislocation ratio and rotor whirling frequency were analyzed using the transient CFD method with the multi-frequency elliptical orbit rotor whirling model. Conclusions are summarized as follows:

(1) The circumferential pressure distribution of the seal varies by following sinusoid approximately. Compared with the conventional LS, the developed NDS has two divergent wedge gaps and reduces hydrodynamic pressure effects, then

effectively decreases the circumferential pressure difference and tangential force (40 %~190 % smaller) of rotor surface.

(2) The magnitude of seal leakage linearly increases with eccentricity ratio and dislocation ratio approximately, and the leakage of the NDS is larger (about 0.9 %~1.5 %) than the conventional LS.

(3) In the same motion amplitude, the response force increases with the increasing rotor whirling frequency, but the response force of the NDS is lower than that of the LS at the same rotor whirling frequency. Meanwhile, the response force of the NDS decreases with the increase of the dislocation ratio.

(4) With the increasing rotor whirling frequency, the direct stiffness coefficients increase while the absolute values of both cross-coupled stiffness coefficients and damping coefficients decrease.

(5) Compared to the LS, the negative dislocated structure of the NDS is effective in decreasing the seal cross-coupled stiffness coefficients (about 28.8 %~206.2 % smaller), increasing effective damping coefficients (about 26.15 %~60.39 % larger) and improving rotor system stability. Therefore, the negative dislocated structure of the seal is more suitable for the stability of rotor system.

The goal of this study was to develop a valuable seal structure design (negative dislocated seal, NDS) and deeply investigate the static and rotordynamic characteristics of the seal, thereby demonstrating that the NDS contributes to the stability of rotor system without the influence on seal performance.

Acknowledgments

This work is supported by the National Natural Science Foundation (Grant Nos. 51675351 and 51605016) and Natural Science Foundation of Liaoning Province, China (Grant No. 20150220113).

Nomenclature

R : Seal radius
r : Rotor radius
δ : The distance between stator center and seal center
ω : Angular frequency of rotor spin
γ : Dislocation ratio
A, B : The major axis of rotor elliptic whirling orbit
Ω : Angular frequency of rotor whirling
f : Rotor whirling frequency
C_r : Seal clearance
x, y : Rotor displacement
$\dot{x}, \dot{y}$: Rotor velocity
F_x, F_y : Response force acting on the rotor
K_{xx}, K_{yy} : Direct stiffness
K_{xy}, K_{yx} : Cross-coupled stiffness
C_{xx}, C_{yy} : Direct damping
C_{xy}, C_{yx} : Cross-coupled damping
D_{xx}, D_{xy} : Rotor motion for x direction excitation
D_{yx}, D_{yy} : Rotor motion for y direction excitation
F_{xx}, F_{xy} : Response force for x direction excitation
F_{yx}, F_{yy} : Response force for y direction excitation
H_{xx}, H_{yy} : Direct force impedance
H_{xy}, H_{yx} : Cross-coupled impedance
C_{eff} : Effective damping

References

[1] D. Sun et al., A trigonometric series expansion based method for the research of static and dynamic characteristics of eccentric seals, *J. of Mechanical Science and Technology*, 28 (6) (2014) 2111-2120.

[2] X. Li, J. Yang and W. Xu, Research and comparison on the leakage and fluid force between the axial and the radial labyrinth seal, *J. of Mechanical Science and Technology*, 29 (11) (2015) 4611-4620.

[3] S. Subramanian, A. S. Sekhar and B. V. S. S. S. Prasad, Influence of combined radial location and growth on the leakage performance of a rotating labyrinth gas turbine seal, *J. of Mechanical Science and Technology*, 29 (6) (2015) 2535-2545.

[4] W. Zhang et al., Comparison of leakage performance and fluid-induced force of turbine tip labyrinth seal and a new kind of radial annular seal, *Computer & Fluids*, 105 (2014) 125-137.

[5] M. Zhang, J. Yang, W. Xu and Y. Xia, Leakage and rotordynamic performance of a mixed labyrinth seal compared with that of a staggered labyrinth seal, *J. of Mechanical Science and Technology*, 31 (5) (2017) 2261-2277.

[6] Z. Li, J. Li and Z. Feng, Numerical comparison of rotordynamic characteristics for a fully-partitioned pocket damper seal and a labyrinth seal with high positive and negative inlet preswirl, *J. of Engineering for Gas Turbine and Power*, 138 (4) (2015) 42505-42515.

[7] J. M. Li, D. C. Pranabesh and K. Frank, Evaluation of centrifugal compressor stability margin and investigation of antiswirl mechanism, *Proceedings of the Thirty-Second Turbomachinery Symposium*, USA (2003) 49-57.

[8] D. Sun, S. Wang, Y. Ai, H. Zhou and K. M. Wang, Experimental investigation of rotordynamic coefficients for the labyrinth seals with and without shunt injection, *J. of Vibroengineering*, 17 (8) (2015) 4289-4300.

[9] K. K. Nielsen, D. W. Childs and C. M. Myllerup, Experimental and theoretical comparison of two swirl brake designs, *J. of Turbomachinery*, 123 (2) (2001) 353-358.

[10] D. Sun, S. Wang, C. W. Fei, Y. Ai and K. M. Wang, Numerical and experimental investigation on the effect of swirl brake on the labyrinth seal, *J. of Engineering for Gas Turbine and Power*, 138 (3) (2015) Manuscript ID: 032507.

[11] B. Leonardo, G. Alberto, B. Andrea, M. Guido and F. Michele, Optimization of swirl brake design and assessment of its stabilizing effect on compressor rotordyanmic performance, *43rd Turbomachinery & 30th Pump Users Symposia*, Houston, TX, USA (2014).

[12] S. Y. Park, *Computational investigation of fluid injection*

applications for the gas labyrinth seal [dissertation], College Station, TX: Texas A&M University (2002).

[13] D. W. Childs, J. E. McLean Jr., M. Zhang and S. P. Arthur, Rotordynamic performance of a negative-swirl brake for a tooth-on-stator labyrinth, *J. of Engineering for Gas Turbine and Power*, 138 (6) (2015) 062505-062505-8.

[14] E. Memmott, Stability of centrifugal compressor by application of tilt pad seals, damper bearings and shunt holes, *Fifth International Conference on Vibrations in Rotating Machinery IMechE*, Bath, England (1992) 99-108.

[15] E. A. Soto and D. W. Childs, Experimental rotordynamic coefficient results for (a) a Labyrinth Seal with and without shunt injection and (b) a honeycomb seal, *J. of Engineering for Gas Turbine and Power*, 121 (1) (1999) 153-159.

[16] G. L. Von Pragenau, *Damping seals for turbomachinery*, Alabama: George C. Marshall Space Flight Center (1982) Report No.: NASA TP-1987.

[17] L. He et al., Experimental investigation of the sealing performance of honeycomb seals, *Chinese J. of Aeronautics*, 14 (1) (2001) 13-17.

[18] Z. Yu and D. W. Childs, A comparison of experimental rotordynamic coefficients and leakage characteristics be-tween hole-pattern gas damper seals and a honeycomb seal, *J. of Engineering for Gas Turbines & Power*, 120 (4) (1997) 778-783.

[19] G. Vannini et al., Labyrinth seal and pocket damper seal high pressure rotordynamic test data, *J. of Engineering for Gas Turbine and Power*, 136 (2) (2014) 022501.

[20] N. Bachschmid, P. Pennacchi and A. Vania, Steam-whirl analysis in a high pressure cylinder of a turbo generator, *Mechanical Systems & Signal Processing*, 22 (1) (2008) 121-132.

[21] Z. Li, J. Li and X. Yan, Multiple frequencies elliptical whirling orbit model and transient RANS solution approach to rotordynamic coefficients of annual gas seals prediction, *J. of Vibration & Acoustics*, 135 (3) (2013) 031005.

[22] T. Hirano, G. Zenglin and R. G. Kirk, Application of computation fluid dynamics analysis for rotating machinery-part II: labyrinth seal analysis, *J. of Engineering for Gas Turbine and Power*, 127 (4) (2005) 820-826.

[23] Z. Li, J. Li and Z. Feng, Comparisons of rotordynamic characteristics predictions for annular gas seals using the transient CFD method based on different single-frequency and multi-frequency rotor whirling models, *J. of Tribology*, 138 (1) (2015) 011701-011701-18.

[24] B. H. Ertas, A. Delgado and G. Vannini, Rotordynamic force coefficients for three types of annular gas seals with inlet preswirl and high differential pressure ratio, *J. of Engineering for Gas Turbines and Power*, 134 (2012) 042503.

[25] X. Yan, J. Li and Z. Feng, Investigations on the rotordynamic characteristics of a hole-pattern seal using transient CFD and periodic circular orbit model, *J. of Vibration and Acoustics*, 133 (4) (2011) 041007.

[26] G. Chochua and T. A. Soulas, Numerical modeling of rotordynamic coefficients for deliberately roughened stator gas annular seals, *J. of Tribology*, 129 (2) (2007) 424-429.

[27] K. K. Nielsen, K. Janck and H. Underbakke, Hole-pattern and honeycomb seal rotordynamic forces: Validation of CFD-based prediction techniques, *J. of Engineering for Gas Turbines and Power*, 134 (12) (2012) 122505.

[28] S. S. Sreedharan and G. Vannini, CFD assessment of rotordynamic coefficients in labyrinth seals, *Turbine Technical Conference and Exposition*, Düsseldorf, Germany (2014) V07BT32A022-V07BT32A022.

[29] J. Li, Z. Li and Z. Feng, Investigations on the rotordynamic coefficients of pocket damper seals using the multi-frequency, one-dimensional, whirling orbit model and RANS solutions, *J. of Engineering for Gas Turbines and Power*, 134 (2012) 102510.

[30] D. W. Childs, Turbomachinery rotordynamics: Phenomena, modeling, and analysis, *Turbomachinery Rotordynamics Phenomena Modeling & Analysis*, 28 (1993) (1993) 262-263.

Dan Sun received his Ph.D. in 2011, from Southeast University, China. He is an Associate Professor at Shenyang Aerospace University, China. His research interests include the theoretical and experimental study on hydrodynamic lubrication and hydrodynamic characteristics of turbine mechanical seals and journal bearings.

Chengwei Fei received his Ph.D. in 2014, from Beihang University (BUAA), China, and then was a Postdoctoral Fellow until 2017, at The Hong Kong Polytechnic University, Hong Kong. Now he is a Professor at Beihang University, China. His research interests include rotor dynamics, structural reliability and health monitoring for aero-engines and aircrafts.